

Image Reconstruction in Electrical Impedance Tomography through 1D-Convolutional Neural Network

Serge Ayme Kouakouo Nomvussi

*Department of Theoretical and Experimental Electrical Engineering
Brno University of Technology
Brno, Czech Republic
244245@vut.cz*

Jan Mikulka

*Department of Theoretical and Experimental Electrical Engineering
Brno University of Technology
Brno, Czech Republic
mikulka@vut.cz*

Abstract—This paper presents a comparative analysis of image reconstruction performance using a 1D-Convolutional Neural Network (1D-CNN) against the Total Variation and the Gauss-Newton methods. The evaluation, conducted across multiple tests conditions, demonstrates that the 1D-CNN consistently outperforms both conventional methods in terms of correlation coefficient and structural similarity index (SSIM). In noise-free scenarios, the 1D-CNN achieves significantly higher correlation and SSIM values, indicating superior reconstruction accuracy. Furthermore, in the presence of noise (30 dB and 60 dB), the performance of the Total Variation and Gauss-Newton methods deteriorates considerably, whereas the 1D-CNN maintains high correlation and SSIM values, demonstrating strong robustness to noise. These findings highlight the effectiveness of deep learning-based approaches for image reconstruction, making the 1D-CNN a promising alternative to traditional reconstruction techniques.

Keywords—1D-convolutional Neural Network, Total Variation, Newton-Gauss, EIT.

I. INTRODUCTION

Electrical Impedance Tomography (EIT) is widely used in biomedical imaging, geophysics, and industrial process monitoring to reconstruct an object's internal conductivity distribution [1-3] based on electrical measurements taken at its boundary. Despite its advantages, EIT is highly ill-posed and sensitive to measurement noise, posing challenges for accurate reconstruction [4]. Traditional reconstruction methods, such as the Gauss-Newton, Total Variation, and back-projection algorithms, require significant computational resources and often produce blurry reconstructions [5-10]. While the Gauss-Newton method performs well in noise-free conditions, its accuracy deteriorates significantly in the presence of noise, limiting its applicability in real-world scenarios [11].

Deep learning has emerged as a promising alternative for EIT image reconstruction, offering improvements in both speed and accuracy [4]. Convolutional Neural Networks (CNNs), in particular, have been extensively applied to image processing tasks. However, most existing deep learning-based EIT methods rely on 2D CNNs, which may not optimally process the inherently sequential 1D voltage measurements acquired in EIT [5]. Given this sequential nature, 1D CNNs provide a more

suitable architecture for feature extraction and conductivity estimation [12].

In this work, we propose a 1D CNN-based approach for EIT image reconstruction that directly maps voltage measurements to conductivity distributions. By leveraging the efficiency of 1D convolutions, our method aims to enhance the performance of the reconstructed images.

II. METHODS

A synthetic dataset was generated using the EIDORS framework [13], a MATLAB-based tool for forward and inverse modeling in EIT. The dataset comprises circular and rectangular targets with varying conductivities (ranging from 0.01 S/m to 0.12 S/m) placed in a water-filled container (0.04 S/m). Electrodes surrounding the container facilitate current injection and voltage measurement, following predefined injection and measurement patterns. The dataset contains 17745 samples, including variations in noise levels introduced through white Gaussian noise. Each sample consists of:

- Train_voltage: [208 x 10647] matrix of voltage measurements.
- Train_conductivity: [1024 x 10647] matrix of conductivity distributions.
- Validation and test datasets: Similar structure with 3549 samples each.

To ensure numerical stability and improve the efficiency of the training process, the data is preprocessed through normalization of both voltage and conductivity values. This normalization mitigates the effects of varying scales and enhances the convergence of the learning algorithm. Each sample contains 208 voltage measurements as input features and 1024 conductivity values as output labels, as mathematically formulated in Equations (1) and (2).

$$U = (U_1, U_2, \dots, U_i) \quad \text{with } i = 1, 2, \dots, 208, \quad (1)$$

$$\sigma = (\sigma_1, \sigma_2, \dots, \sigma_j) \quad \text{with } j = 1, 2, \dots, 1024. \quad (2)$$

The proposed one-dimensional (1D) Convolutional Neural Network (CNN) architecture comprises four key components: an input layer, a hierarchical feature extraction mechanism utilizing convolutional layers, a flatten layer for dimensionality reduction, and a series of fully connected layers for conductivity estimation. A detailed structural representation of the network is shown in Fig. 1.

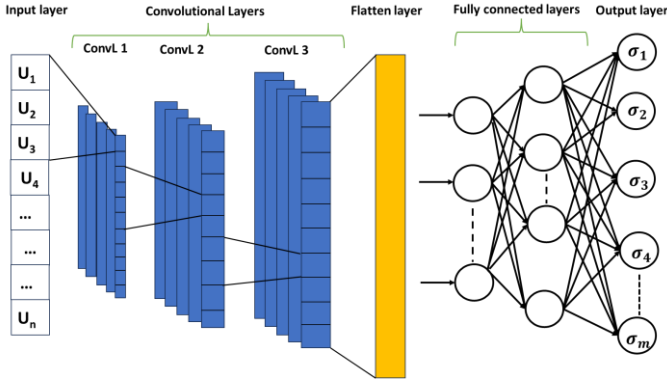


Fig. 1. Architecture of the new method

The network begins with a sequence input layer of size 208, corresponding to the number of voltage measurements per sample. This layer ensures that the spatial and temporal relationships among the voltage readings are preserved, allowing the model to effectively capture meaningful patterns.

Feature extraction in this model is accomplished through a series of three 1D convolutional layers (ConvL), each designed to progressively learn higher-level representations from the input data. These convolutional layers use a kernel size of 3, ensuring a localized receptive field that captures important patterns and dependencies. The first convolutional layer (ConvL 1) uses 128 filters, enabling the extraction of fundamental low-level features. As the network deepens, the second convolutional layer (ConvL 2) increases to 256 filters, enabling the model to learn more complex patterns. Finally, the third convolutional layer (ConvL 3) uses 1024 filters, significantly boosting the capacity of the network to capture intricate and abstract high-level representations.

To improve training stability and efficiency, each convolutional layer is followed by a Batch Normalization (BN) layer. Batch normalization normalizes activations, reducing internal covariate shifts to stabilize training and accelerate convergence. It also serves as a form of regularization, enhancing the model's generalization performance. After batch normalization, a Rectified Linear Unit (ReLU) activation function is applied to introduce non-linearity. The ReLU function, mathematically defined as:

$$f(U) = \max(0, U). \quad (3)$$

This ReLU function ensures that all negative values are set to zero, while positive values remain unchanged. This non-linear transformation helps the network learn complex representations and mitigates the vanishing gradient problem, which can hinder deep networks from learning effectively. By combining convolutional layers, batch normalization, and ReLU activation, the model effectively extracts hierarchical features, facilitating robust and efficient learning.

After the convolutional layers have extracted hierarchical features from the input data, a flatten layer is applied to transform the multi-dimensional feature maps into a one-dimensional vector. This transformation is essential, as it enables the transition from convolutional operations to fully connected layers, which operate on flattened representations. By preserving the extracted spatial features while restructuring them into a linear form, the flattening process ensures that the network can effectively process the learned patterns in subsequent layers.

After this, the extracted features are refined and interpreted through a series of fully connected layers (FCLs), which are essential for mapping the learned representations to the final output. The first fully connected layer (FCL 1) has 128 neurons, allowing the model to integrate low-level features into more meaningful representations. The second fully connected layer (FCL 2) follows, with 256 neurons, further increasing the network's capacity to model complex relationships. The third and final fully connected layer (FCL 3) has 1024 neurons, enabling a deep, highly expressive feature space that captures intricate dependencies. Each fully connected layer is followed by a ReLU activation function to enhance the model's learning capacity.

The final stage of the network predicts conductivity values, with the last fully connected layer containing 1024 neurons. Each neuron represents a predicted conductivity value, capturing the underlying spatial relationships learned from the input data. A regression layer is applied at the output to ensure the final prediction is suitable for regression tasks. This layer computes the final conductivity map, representing the model's estimated conductivity values across the input domain.

To optimize the learning process and improve the network's performance, we use the Adam optimizer, a popular choice for deep learning applications due to its ability to adapt the learning rate and incorporate momentum. This makes Adam particularly effective in navigating the complex loss landscapes of deep networks, ensuring efficient training. The training process uses several key hyperparameters: L2 regularization is set to 0.0002,

helping prevent overfitting by penalizing large weights and promoting generalization. The mini-batch size is set to 16, allowing the model to process data in manageable chunks while maintaining computational efficiency. Training is set to run for a maximum of 1000 epochs, providing ample time for the network to converge. The initial learning rate is set at 0.0005, providing a balance between making significant progress and allowing for fine-tuning over time. During training, the performance of the model is validated every 5 epochs, ensuring that progress is monitored, and adjustments can be made. To avoid overfitting and ensure generalization, early stopping is implemented: if validation loss does not improve for 10 consecutive steps, training halts to prevent unnecessary computation.

The performance of the model is evaluated using the Mean Squared Error (MSE) loss function, which measures the average squared differences between the predicted conductivity values T_i and the true values Y_i . The MSE is defined as:

$$MSE = \frac{1}{N} \sum_{i=1}^M (Y_i - T_i)^2. \quad (4)$$

The correlation coefficient (Corr), as calculated in Equation (5), is a crucial metric for assessing the degree of correlation between the recovered image Y_{mn}^* and the original image Y_{mn} . This coefficient provides insights into the strength of the correlation, offering a quantitative measure of the quality of the reconstructed conductivity map. The correlation coefficient is instrumental in discerning how well the recovered image aligns with the original image. The parameters $\overline{Y_{mn}^*}$ and $\overline{Y_{mn}}$ represent the mean values of the recovered and original images, respectively.

$$\text{corr} = \frac{\sum_m \sum_n (Y_{mn}^* - \overline{Y_{mn}^*})(Y_{mn} - \overline{Y_{mn}})}{\sqrt{(\sum_m \sum_n (Y_{mn}^* - \overline{Y_{mn}^*})^2)(\sum_m \sum_n (Y_{mn} - \overline{Y_{mn}})^2)}}. \quad (5)$$

The structural similarity index (SSIM), formulated in Equation (5), is a perceptual metric that assesses the quality of the reconstructed image by considering luminance, contrast, and structural fidelity. Unlike traditional error-based metrics, SSIM evaluates image similarity based on structural content, making it more aligned with human visual perception. An SSIM value of 1 indicates perfect structural similarity between the original and reconstructed images, while values below 1 suggest variations in image quality.

$$\text{ssim}(x, y) = \frac{(2\mu_x\mu_y + C_1)(2\sigma_{xy} + C_2)}{(\mu_x^2 + \mu_y^2 + C_1)(\sigma_x^2 + \sigma_y^2 + C_2)}, \quad (6)$$

where $\mu_x, \mu_y, \sigma_x, \sigma_y$ and σ_{xy} are the local means, standard deviations, and cross-covariance for images x, y . C_1 and C_2 are small constant which prevent division by zero.

III. RESULTS

The training and validation loss values recorded over multiple epochs illustrate the model's learning progression and generalization capability, as shown in Fig. 2. Initially, both losses were high, starting at 56.9 (training) and 41.6 (validation) at epoch 1. A rapid decline is observed during the early stages, with losses significantly reducing by epoch 50 (training: 33.2, validation: 32.1), indicating effective learning. However, after approximately 100 epochs, the validation loss reduction slows and stabilizes around 25.15 from epoch 400 onward, while the training loss continues to decrease, reaching 5.34 at epoch 495. This growing discrepancy suggests potential overfitting, where the model continues to improve on the training data but no longer generalizes effectively to unseen data. These results highlight the importance of implementing early stopping or regularization techniques to balance training performance and generalization ability.

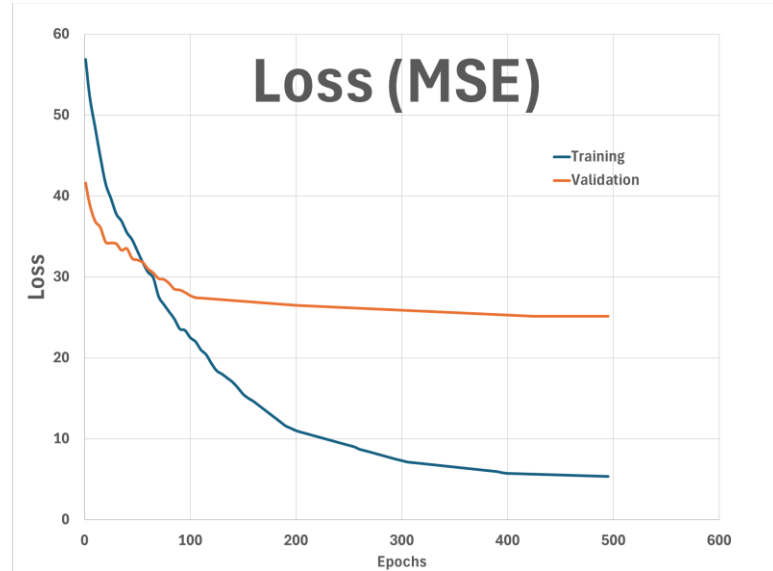
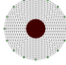
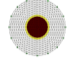
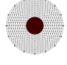
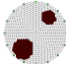

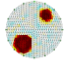
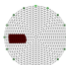
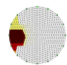
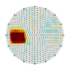

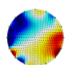
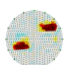

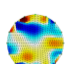
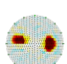


Fig. 2. Loss of the new 1D-CNN proposed method

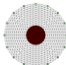
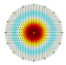
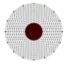
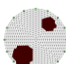
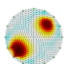
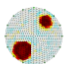
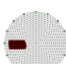
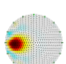
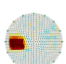

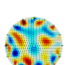
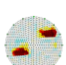

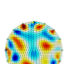
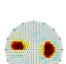
TABLE I. COMPARISON NEW METHOD AND TOTAL VARIATION

Position / Noise	Model	Reconstructed image Total Variation algorithm	Reconstructed image with 1D-CNN
1/No		 corr = 0.627 ssim = 0.964	 corr = 0.967 ssim = 0.989
2/No		 corr = 0.795 ssim = 0.612	 corr = 0.978 ssim = 0.631
3/No		 corr = 0.608 ssim = 0.555	 corr = 0.721 ssim = 0.591
4/Yes 60 dB		 corr = 0.070 ssim = 0.542	 corr = 0.927 ssim = 0.614
5/Yes 30 dB		 corr = 0.046 ssim = 0.489	 corr = 0.951 ssim = 0.617

The results in Table I demonstrate that the proposed 1D-CNN consistently outperforms the Total Variation (TV) method across all tested conditions, both in noise-free and noisy scenarios. In the absence of noise (Positions 1–3), the 1D-CNN achieves higher correlation coefficients (0.967, 0.978, and 0.721) and SSIM values (0.989, 0.631, and 0.591) compared to the TV algorithm (correlation: 0.627, 0.795, 0.608; SSIM: 0.964, 0.612, 0.555), indicating superior reconstruction accuracy. The performance gap becomes more pronounced in the presence of noise at 60 dB and 30 dB (Positions 4–5), where the TV algorithm exhibits a substantial decline, with correlation

dropping to 0.070 and 0.046, respectively, while the 1D-CNN maintains significantly higher correlation values of 0.927 and 0.951. Similarly, the SSIM values for the TV algorithm (0.542 and 0.489) remain lower than those of the 1D-CNN (0.614 and 0.617), underscoring the latter’s robustness to noise. These findings highlight the superior performance of the 1D-CNN in reconstructing images with higher fidelity and resilience to noise, making it a more effective approach than the traditional TV algorithm.

TABLE II. COMPARISON NEW METHOD AND GAUSS-NEWTON

Position / Noise	Model	Reconstructed image Gauss-Newton algorithm	Reconstructed image with 1D-CNN
1/No		 corr = 0.703 ssim = 0.929	 corr = 0.967 ssim = 0.989
2/No		 corr = 0.455 ssim = 0.609	 corr = 0.978 ssim = 0.631
3/No		 corr = 0.38 ssim = 0.512	 corr = 0.915 ssim = 0.591
4/yes 30 dB		 corr = 0.071 ssim = 0.601	 corr = 0.927 ssim = 0.614
5/Yes 60 dB		 corr = 0.052 ssim = 0.561	 corr = 0.951 ssim = 0.617

The results in Table II demonstrate that the proposed 1D-CNN consistently outperforms the Gauss-Newton algorithm across all tested conditions, including both noise-free and noisy scenarios. Under noise-free conditions (Positions 1–3), the 1D-CNN achieves significantly higher correlation coefficients (0.967, 0.978, and 0.915) and SSIM values (0.989, 0.631, and 0.591) compared to the Gauss-Newton algorithm (correlation: 0.703, 0.455, 0.38; SSIM: 0.929, 0.609, 0.512), highlighting its superior reconstruction accuracy. The disparity in performance becomes even more evident under noisy conditions at 30 dB and 60 dB (Positions 4–5), where the Gauss-Newton algorithm experiences a substantial degradation in correlation (0.071 and 0.052) and SSIM (0.601 and 0.561). In contrast, the 1D-CNN maintains significantly higher correlation values (0.927 and 0.951) and SSIM scores (0.614 and 0.617), demonstrating its robustness to noise. These results confirm that the 1D-CNN is more effective than the Gauss-Newton algorithm in preserving structural details and maintaining high-fidelity image reconstruction, particularly under noisy conditions.

IV. DISCUSSION

The results of this study confirm that the proposed 1D-CNN outperforms the Total Variation and the Gauss-Newton methods in all tested conditions. In noise-free scenarios, the 1D-CNN consistently achieves higher correlation coefficients and SSIM values, indicating superior image reconstruction quality. While both the TV and Gauss-Newton algorithms show moderate performance in the absence of noise, their effectiveness significantly declines in the presence of noise, particularly at 30 dB and 60 dB. The TV algorithm exhibits a drastic drop in correlation, reaching as low as 0.046 under 30 dB noise, while the Gauss-Newton algorithm performs similarly poorly, with a correlation of 0.052 under 60 dB noise. In contrast, the 1D-CNN maintains high correlation values (above 0.9) and relatively stable SSIM scores, demonstrating its strong resilience to noise. These findings suggest that deep learning-based methods, such as the 1D-CNN, provide significant advantages in image reconstruction, particularly in noisy environments where traditional techniques fail. The results highlight the potential of CNN-based approaches to improve reconstruction accuracy in practical applications, such as medical imaging, signal processing, and remote sensing, where robustness to noise is critical. Future work will explore the optimization of network architectures and the application of 1D-CNN models to more complex reconstruction tasks.

ACKNOWLEDGMENT

The author, S. Kouakouo, extends gratitude to the Department of Theoretical and Experimental Electrical Engineering. The completion of this work would not have been possible without the invaluable guidance

REFERENCES

- [1] Harikumar, R. Prabu, and S. Raghavan, "Electrical impedance tomography (EIT) and its medical applications: a review," *Int. J. Soft Comput. Eng.*, vol. 3, no. 4, pp. 193–198, 2013.
- [2] A. Adler and D. Holder, Eds., *Electrical Impedance Tomography: Methods, History and Applications*. Boca Raton, FL, USA: CRC Press, 2021.
- [3] A. Adler and R. Guardo, "Electrical impedance tomography: regularized imaging and contrast detection," *IEEE Trans. Med. Imaging*, vol. 15, no. 2, pp. 170–179, 1996.
- [4] T. Zhang, M. Hirano, K. Oka, and Y. Tagawa, "Advances of deep learning in electrical impedance tomography image reconstruction," *Front. Bioeng. Biotechnol.*, vol. 10, Art. no. 1019531, 2022.
- [5] R. Hrabuska, P. Dostal, V. Vasicek, and P. Kromer, "Image reconstruction for electrical impedance tomography: Experimental comparison of radial basis neural network and Gauss–Newton method," *IFAC-PapersOnLine*, vol. 51, no. 6, pp. 438–443, 2018.
- [6] T. Zhang, M. Hirano, K. Oka, and Y. Tagawa, "Advances of deep learning in electrical impedance tomography image reconstruction," *Front. Bioeng. Biotechnol.*, vol. 10, Art. no. 1019531, 2022.
- [7] T. A. Khan, S. H. Ling, and A. A. Rizvi, "Optimisation of electrical impedance tomography image reconstruction error using heuristic algorithms," *Artif. Intell. Rev.*, vol. 56, no. 12, pp. 15079–15099, 2023.
- [8] M. R. Islam and M. A. Kiber, "Electrical impedance tomography imaging using Gauss-Newton algorithm," in *Proc. Int. Conf. Informatics, Electron. Vis. (ICIEV)*, Dhaka, Bangladesh, 2014, pp. 1–5.
- [9] M. Farha, "Combined algorithm of total variation and Gauss-Newton for image reconstruction in two-dimensional electrical impedance tomography (EIT)," in *Proc. Int. Sem. Sensors, Instrum., Meas. Metrol. (ISSIMM)*, Bandung, Indonesia, 2017, pp. 25–29.
- [10] L. I. Rudin, S. Osher, and E. Fatemi, "Nonlinear total variation based noise removal algorithms," *Physica D: Nonlinear Phenom.*, vol. 60, no. 1–4, pp. 259–268, 1992.
- [11] S. A. K. Nomvussi and J. Mikulka, "Enhanced image reconstruction in electrical impedance tomography using radial basis function neural networks," *Meas. Sci. Rev.*, vol. 24, no. 6, pp. 200–210, 2024.
- [12] X. Li, X. Liu, B. Zhao, Y. Zhou, and G. Wang, "One-dimensional convolutional neural network (1D-CNN) image reconstruction for electrical impedance tomography," *Rev. Sci. Instrum.*, vol. 91, no. 12, pp. 1–7, 2020.
- [13] A. Adler and W. R. B. Lionheart, "Uses and abuses of EIDORS: An extensible software base for EIT," *Physiol. Meas.*, vol. 27, no. 5, pp. S25–S42, 2006.